Diss. ETH No. 13427

Electron Interferometry

A dissertation submitted to the
SWISS FEDERAL INSTITUTE OF TECHNOLOGY
ZÜRICH

for the degree of
Doctor of Natural Sciences

presented by

STEFAN EGGER
Dipl. Phys. ETH
born on March 25, 1969
citizen of Thal (St.Gallen)

accepted on the recommendation of

Prof. Dr. Danilo Pescia, examiner
Prof. Dr. Hans-Christoph Siegmann, co-examiner

2000

Contents

Abstract

Spin polarized low energy electrons with well-defined energy and direction are injected into a spin polarized Cu/Co/Cu(100) quantum well structure. The intensity of the specularly reflected beam oscillates as a function of the Cu thickness, indicating that the quantum well acts as a Fabry-Pérot type interferometer. The spin resolved intensities are phase shifted, proving spin selectivity of the interferometer. The period diverges when the electron energy approaches a band edge.

Interlayer exchange coupling (IXC) has been investigated with magneto-optical Kerr effect on the Co/Cu system. We find a surprising strong temperature dependence. A non magnetic cap layer produces pronounced oscillations of the IXC with periods of 2.5 and 5.5 atomic layers (AL). The oscillations are strong enough to switch the coupling from ferromagnetic to antiferromagnetic and vice-versa. The Co film thickness strongly affects the IXC as well, with a period of 2 AL.

Zusammenfassung

Wir streuen niederenergetische, spinpolarisierte Elektronen mit bekannter Energie und Richtung an einer magnetisierten Cu/Co/Cu(100)-Quantentopfstruktur. Die Intensität des spiegelnd reflektierten Strahls oszilliert als Funktion der Cu-Dicke, was zeigt, dass der Quantentopf ein Fabry-Pérot-Interferometer für Elektronen bildet. Die spinaufgelösten Intensitäten sind phasenverschoben, was die Spinabhängigkeit des Interferometers beweist. Die Periode divergiert, wenn sich die Elektronenenergie einem Bandrand nähert.

Mit magneto-optischem Kerreffekt wird die Zwischenschicht-Austauschkopplung (IXC) am Co/Cu-System untersucht. Wir finden eine überraschend grosse Temperaturabhängigkeit. Eine nichtmagnetische Deckschicht erzeugt Oszillationen der IXC mit Perioden von 2.5 und 5.5 Atomlagen (AL). Die Oszillationen sind stark genug, um die Kopplung zwischen ferromagnetisch und antiferromagnetisch mehrmals zu wechseln. Die Co-Filmdicke beeinflusst ebenfalls stark die IXC, mit einer Periode von 2 AL.

Introduction

Atomically thin magnetic films have special properties. Because of their small thickness, electron interference occurs. In addition, the interference process is spin dependent. In this thesis, two different electron interference effects are studied. In *chapter 3* we investigate the interaction of a *polarized* electron beam with a magnetic quantum well. This study produces a picture of the electron wave function in a quantum well. The experimental technique is spin polarized low energy electron diffraction. We extend a model by Loly and Pendry to explain our experimental data and discuss its implication for interlayer exchange coupling (IXC). A detailed study of interlayer exchange coupling is presented in *chapter 4*. Magneto-optical Kerr effect was used to perform experiments. We studied the influence of temperature, of a cap layer and of magnetic layer thicknesses on IXC. For our study, we have used a multilayer structure based on Co and Cu grown epitaxially on Cu(100). As Cu has a relatively simple Fermi surface, it is possible to compare experimental results with theoretical models.

We start with a brief description of the experimental techniques used (*chapter 1*). In *chapter 2* we give some facts about sample preparation.

Chapter 1

Experimental Techniques

1.1 MOKE

Magneto-optical Kerr effect (MOKE) in the transversal geometry was used (see Fig. 1.1) to investigate the in-plane magnetization. Linearly

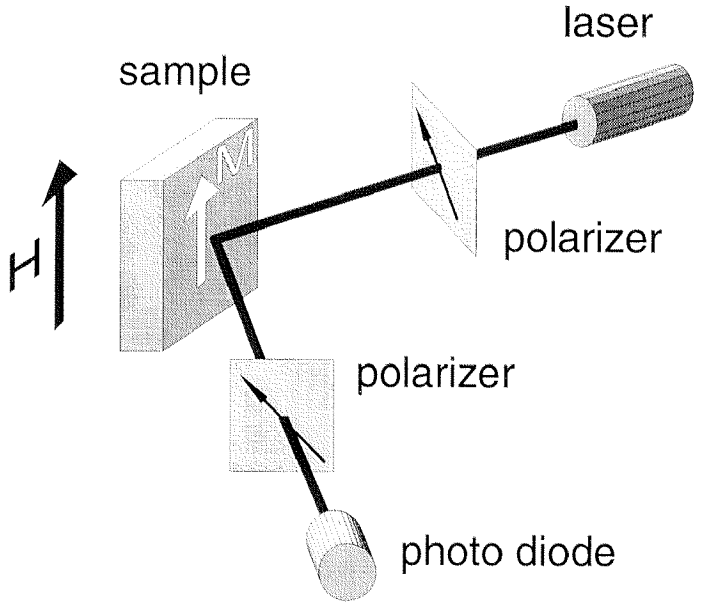

Figure 1.1: *Schematic MOKE setup.*

polarized light reflected at the sample passes a second polarizer and goes in a photo diode. The change of the reflected intensity, when the magnetic field is switched, is proportional to the magnetization. It is

about 0.01% for an atomically thin film. MOKE measures the total magnetic moment over about 100 surface atomic layers.

We used a diode laser with 635 nm wave length. For measurements on wedge structures the laser beam can be focused. The spot size is 35 μm. The hysteresis loops in Fig. 1.2 are the averages over ten sweeps.

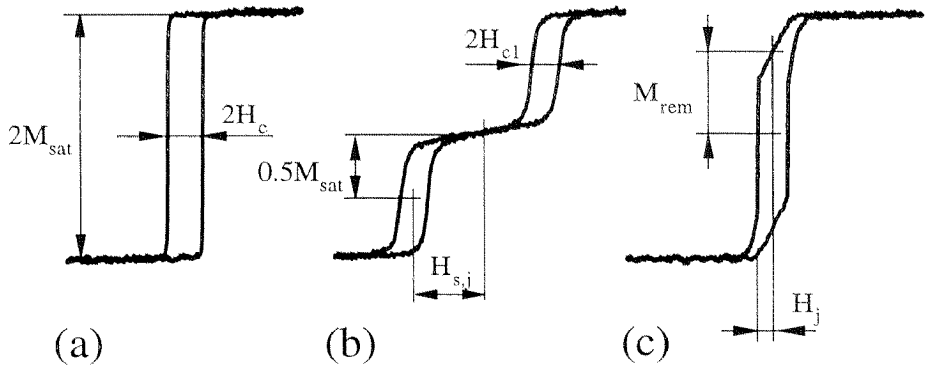

Figure 1.2: *Three typical hysteresis loops: a) Square loop, b) loop shifted by anisotropy or antiferromagnetic coupling, c) loop shifted by antiferromagnetic coupling.*

1.2 SPLEED

Spin polarized low energy electron diffraction [1] (SPLEED) is a very surface sensitive tool. The probing depth for low energy electrons is about 3 AL. The sketch in Fig. 1.3 shows the SPLEED experiment. As a source of polarized electrons we used a strained GaAs crystal. To achieve negative electron affinity Cs and O_2 was deposited before use. We irradiate the source with circularly polarized light from a diode laser. Longitudinal spin polarized electrons are photo emitted. This electrons are deflected by 90° in order to obtain a transversal polarized beam at the sample. The beam polarization can be switched by changing the handiness of the laser light with a Pockels cell used as a $\lambda/4$ retarder. In the SPLEED experiment, the sample is magnetized by a field pulse. The magnetic field is switched off and the number of elastically reflected electrons is counted, for incident electrons with spin parallel and antiparallel to the magnetization. This gives us the

spin asymmetry

$$A \equiv \frac{1}{P_0} \cdot \frac{R_{\text{up}} - R_{\text{down}}}{R_{\text{up}} + R_{\text{down}}}$$

with P_0 being the spin polarization of the incoming electron beam, in our case $P_0 \approx 40\%$. All measurements were done with a fixed angle of incidence of 20° with respect to the surface normal. The electron energy resolution is about 1 eV. Typically, we count half a million electrons per data point: this gives us good statistics.

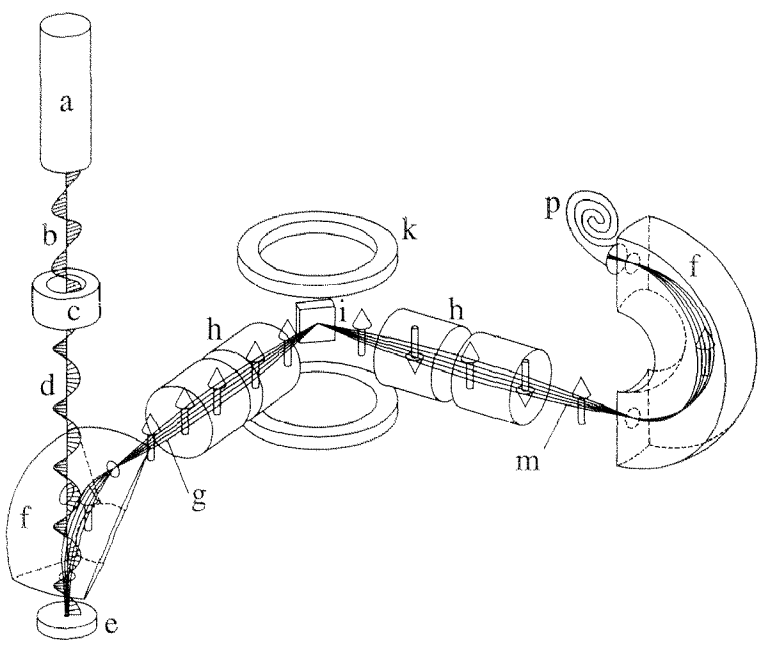

Figure 1.3: *Spin polarized low energy electron diffraction: a) diode laser (λ=785 nm, $\hbar\omega$=1.58 eV), b) linear polarized light, c) Pockels cell, d) circularly polarized light, e) GaAs crystal, f) energy analyzer, g) polarized electron beam, h) electro-static lenses, i) sample, k) coil, m) reflected electron beam, p) channeltron.*

1.3 STM

For checking the quality of the surface substrate and the epitaxial films we used, in addition to LEED and Auger spectroscopy, a home made room temperature scanning tunneling microscope (STM) with electrochemically etched tungsten tips [2].

Chapter 2

Sample Preparation

The experiments were performed with the sample in ultra-high vacuum (UHV) at a base pressure of $3 \cdot 10^{-11}$ mbar. We can characterize the sample with low energy electron diffraction (LEED), Auger electron spectroscopy (AES) and scanning tunneling microscopy (STM).

Our substrate is a copper single crystal. The surface is mechanically and electro-chemically polished and has a miscut of 0.7° with respect to the (100)-plain. The miscut induces steps parallel to the $[1\bar{1}0]$-direction. After sputtering with argon ions and annealing at ≈ 500°C the surface is flat on an atomic scale and the steps are visible by scanning tunneling microscopy (for STM micrographs see [3]).

Thin films were grown by molecular beam epitaxy (MBE) at about $2 \cdot 10^{-10}$ mbar pressure. The rate of deposition was controlled be a quartz balance and by Auger spectroscopy [4]. We worked with deposition rates between 0.1 and 0.6 atomic layers (AL) per minute.

2.1 Growing Co on Cu(100)

Cobalt on copper grows in a fcc lattice (bulk Co: hcp). Ramsperger *et al.* [4] have shown the first atomic layers (AL) grow epitaxially, almost layer by layer. The size and shape of the two-dimensional islands responsible for the layer-by-layer growth depends on the growth temperature [3]. Thicker films ($\approx$ 14 AL) show dislocations induced by the mismatch of the lattice constants (the next neighbor distance in hcp bulk Co is approximately 2% smaller then in fcc Cu). In the STM micrographs, dislocation lines along the (110) and $(1\bar{1}0)$-direction are visible (see Fig.2.1). The formation of these lines changes the magnetic properties [5].

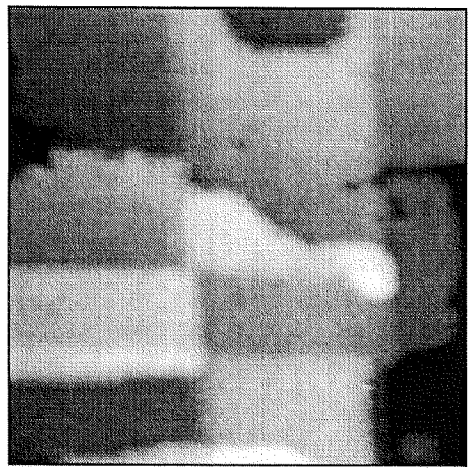

Figure 2.1: *STM micrograph, 25 AL Co on Cu(100), 200 Å x 200 Å, tunneling current 0.26 nA, sample voltage 0.59 V.*

2.2 Growing Cu on Co/Cu(100)

As described by Würsch *et al.* [6] the morphology of a copper film grown on a Co/Cu(100) structure depends on the temperature at deposition: At room temperature there are little pyramids some atomic layers high. The average roughness is about 3 atomic layers. If the sample is cooled at to $-120°C$ during growth, the films are almost perfectly flat.

Chapter 3

Spin Selective Interferometry

Quantum interference of electron waves in Fabry-Pérot-type solid-state resonators has been observed in a number of quantum well structures. The applications of this phenomenon include quantum-well based semiconductor devices [7], accurate mapping of the band structure of solids and surfaces [8, 9, 10, 11, 12, 13] and visualizing the spatial dependence of quantum mechanical wave functions by means of scanning tunneling spectroscopy (STS) [12, 13, 14]. In the experiment presented in this chapter we demonstrate that the Fabry-Pérot quantum well resonator can be made spin selective [15].

The Cu/Co films were grown by molecular beam epitaxy at room temperature on top of a Cu(100) single crystal. First we grow a Co film of 5 atomic layers (AL) thickness followed by a Cu cap layer. During film growth we perform two experiments simultaneously: magneto-optic Kerr effect (MOKE) [6] and spin polarized low energy electron Diffraction (SPLEED). MOKE is used to determine the thickness of the various films. Oscillations at the coercive field, probed with the Kerr effect, give the thickness calibration. The period of these oscillations is 1 AL for a Co layer grown on Cu [16] and 2.5 ± 0.2 AL for a Cu layer grown on top of a Co layer [6] (oscillations see Fig. A.1, p. 38).

3.1 Spin Asymmetry

The resonator consists of a Cu film of variable thickness d_{Cu} covering an in-plane magnetized Co film [6]. Low energy electrons are injected into the resonator from the vacuum side. Apart from having a well defined energy and direction, they are spin polarized, with polarization parallel (up) or antiparallel (down) to the magnetization of the Co

film. Some electrons are specularly reflected at the same energy: the specularly reflected intensities $R_{\mathrm{up(down)}}$ are measured separately for each spin channel [17] as a function of the film thickness d_{Cu}. We define a spin asymmetry as $A \equiv 1/P_0 \cdot (R_{\mathrm{up}} - R_{\mathrm{down}})/(R_{\mathrm{up}} + R_{\mathrm{down}})$ [17], P_0 being the spin polarization of the incoming electron beam, in our case $P_0 \approx 40\%$.

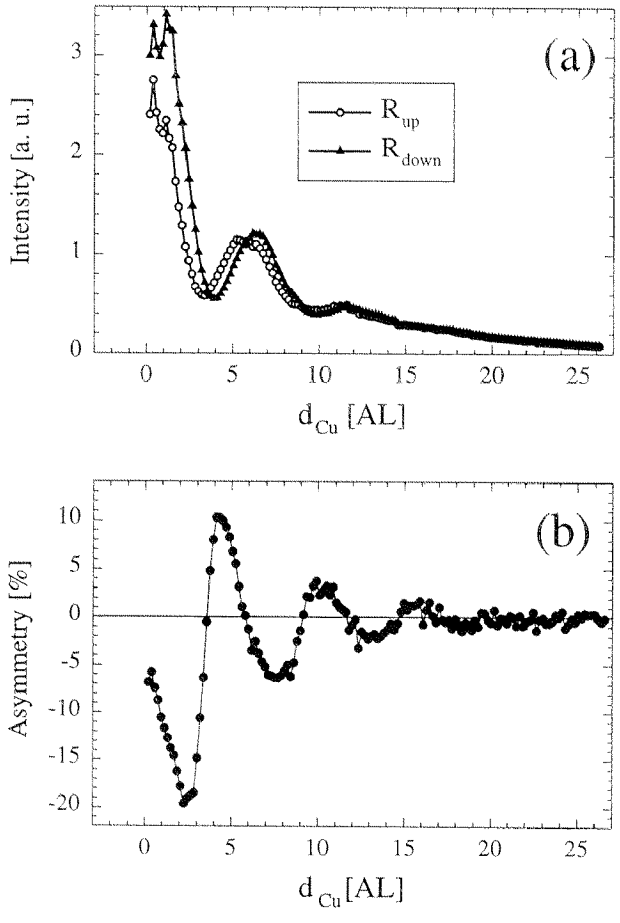

Figure 3.1: *a) Oscillatory behavior of the experimental specularly reflected intensities $R_{\mathrm{up(down)}}$ as a function of the resonator thickness for the two spin channels. $R_{\mathrm{up(down)}}(d_{\mathrm{Cu}})$ were measured in real time during growth. Electron energy: 10.8 eV. The underlying Co film was $\approx$ 5 AL thick. b) Spin asymmetry as a function of d_{Cu}, obtained from Fig. 3.1a.*

Fig. 3.1a shows $R_{\mathrm{up(down)}}$ as a function of d_{Cu} at a fixed energy of 12.8 eV and an angle of incidence of 20°. Both curves have one single oscillatory component with the same period. In addition, $R_{\mathrm{up}}(d_{\mathrm{Cu}})$ is

shifted with respect to $R_{\mathrm{down}}(d_{\mathrm{Cu}})$. This shift is provided by the spin dependent potential at the Co-Cu interface. As a consequence of this spin dependent shift the spin asymmetry $A \equiv (R_{\mathrm{up}} - R_{\mathrm{down}})/(R_{\mathrm{up}} + R_{\mathrm{down}})$ shows pronounced up-down oscillations as a function of d_{Cu} [18], which are the fingerprint of spin dependent quantum interference [19].

3.2 Model Proposed by Loly and Pendry

Spin dependent quantum interference can be understood within the model proposed by Loly and Pendry (LP) [20]. In this model, a Bloch electron is confined along one spatial direction within a thin film N AL thick. The confining potential barrier is taken, by the way of illustration, to be infinite. In the limit $N \to \infty$ electron states can be labeled by a Bloch vector $\vec{k}$. In the direction of confinement $\vec{k}$ assumes all values in the range $[-k_{Bz}, k_{Bz}]$, where k_{Bz} defines the boundary of the first Brillouin zone. In this limit, the possible energy levels form energy bands. When N has finite values, only a discrete set of equally spaced k values is allowed in the direction of confinement, the spacing being equal to $\pi/(N \cdot a)$ (a = interlayer spacing). This causes the energy bands to collapse onto a discrete set of allowed energy values, known as quantum well states (QWS) [10, 11, 21], see Fig. 3.2. The potential barriers on both sides of the resonator can be lowered, e.g. by terminating the film on one side with vacuum and on the other with a substrate. QWS located above the vacuum energy become quantum well resonances [19, 21], that is they form, within a continuum spectrum, a discrete set of energies at which electrons can be preferentially injected into the resonator [21, 22, 23]. When N is increased, the allowed k values move toward the nearest Brillouin zone boundary to accommodate more states within the finite interval $[0, k_{Bz}]$, see Fig. 3.2.

Correspondingly, the allowed energy levels drift toward the nearest band edge — with the exception of the band edges themselves, which are pinned by the crystal potential. As a consequence of this movement, allowed energy states will enter periodically a given energy level E when N is varied, thus producing the oscillatory component reported in Fig. 3.1a. Let us now suppose that the substrate side of the resonator is magnetically active. This potential barrier is spin dependent [24, 25]. The wave function reflected at this potential barrier suffers a spin dependent phase shift: this is the origin of the shift observed in Fig. 3.1a. Note that the same quantum well can be used for spin

selection. Let us assume injecting a beam of unpolarized electrons into the resonator. Spin up electrons might be poorly reflected back — say at a minimum of $R_{\mathrm{up}}(d_{\mathrm{Cu}})$. Because of the shift, spin-down electrons are more efficiently reflected and as a result the reflected beam is spin polarized, and its spin polarization can be modulated by varying d_{Cu}.

Within the LP model, one can calculate the oscillation period: in the following we label the theoretically expected period Λ^{LP}. When N is varied, QWS move depending on their distance from the Brillouin

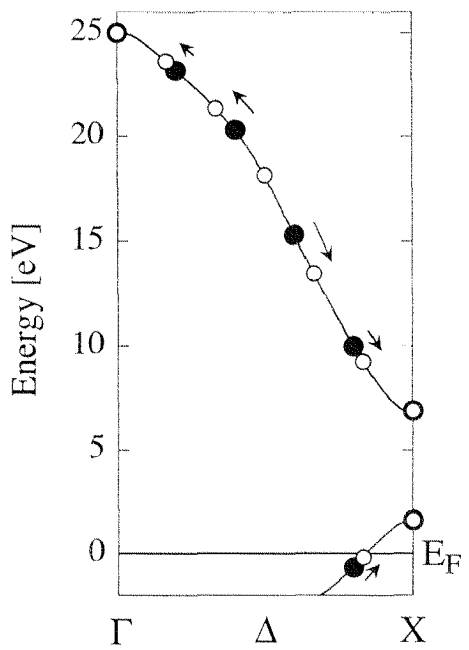

Figure 3.2: *An interferometer model for Bloch electrons. The figure shows the calculated band structure of Cu along the* Δ *direction. The origin of the energy scale is the Fermi level* E_F*. For simplicity, only one unoccupied band is shown: this band is the only unoccupied one along* Δ *below* $E \approx 16$ *eV. Our calculations place the position of the bottom of this band at* ≈ 7 *eV, while experiments [10] (ours included) find the bottom at about 8 eV. Our experiments are performed 20° off the* Δ *direction, but numerical LEED calculations, which take explicitely this offset into account [26], indicate the presence of a similar unoccupied band along the direction probed by the experiment. If Cu has a finite thickness, quantized levels (black dots) are produced, which, following the arrows, approach the nearest zone edge when the thickness is increased and take the position indicated by the open circles.*

zone boundary, see Fig. 3.2. To find the period Λ^{LP}, we equal the distance between two consecutive black dots, calculated by LP to be

$$\frac{\partial E}{\partial k} \cdot \frac{\pi}{Na}$$

with the change in energy produced by varying N, which we calculate to be

$$\frac{\partial E}{\partial k} \cdot \frac{1}{Na} \cdot (k(E) - k_{Bz}) \cdot \Lambda^{\mathrm{LP}}.$$

This leads to the equation

$$\Lambda^{\mathrm{LP}} = \pi/(k(E) - k_{Bz}). \tag{3.1}$$

This equation explicitely shows that the theoretically expected Λ^{LP} is energy dependent, i.e. $\Lambda^{\mathrm{LP}} = \Lambda^{\mathrm{LP}}(E)$, and contains the pinning of the band edges by the crystal potential when N is changed, leading to a singular behavior of the period at the zone boundary [27].

3.3 Experimental Determination of the Period

Fig. 3.3a reports $A(d_{\mathrm{Cu}})$ measured at different electron energies E. Each plot contains one single period $\Lambda(E)$ which increases when E is decreased. At $E \approx 7.5$ eV the period is too large to be determined. A similar energy dependence is apparent from the plots of Fig. 3.3b, which summarize the results of numerical full dynamical layer-dependent LEED and spin polarized LEED calculations [19] for a system consisting of N Cu layers on top of a semi-infinite fcc Co(001) crystal, with $N = 0, 1, 2, 3, 4$ [26, 29]. The experimental $\Lambda(E)$ (Fig. 3.4), obtained from Fig. 3.3a, shows the two important features predicted by the LP model:

i) a divergence at $E_0 \approx 8.1$ eV — that is in the range of energies where an unoccupied band of Cu meets the zone boundary, see Fig. 3.2 and

ii) a functional dependence of $\Lambda(E)$ which agrees with the one expected from the LP model. In fact, near the zone boundary, $(k(E) - k_{Bz}) \propto (E - E_{Bz})^{1/2}$ [30]. Thus, $\Lambda^{\mathrm{LP}}(E) \propto (E - E_{Bz})^{\beta}$ with the power law exponent $\beta = -1/2$. We find that the experimental $\Lambda(E)$ plotted as $\log(\Lambda)$ versus $\log(E - E_0)$ is best fitted by a straight line with $E_0 = 8.1$ eV and slope $-0.6^{+0.1}_{-0.2}$, see inset in Fig. 3.4. The uncertainty

in the determination of the slope is due to the fact that the value of E_0 is only known to be found in the range from 7.5 eV to 8.3 eV, see Fig. 3.3.

A curve similar to Fig. 3.4 is also observed when a Co film of variable thickness is deposited on top of a Cu(100) crystal, see Fig. 3.5.

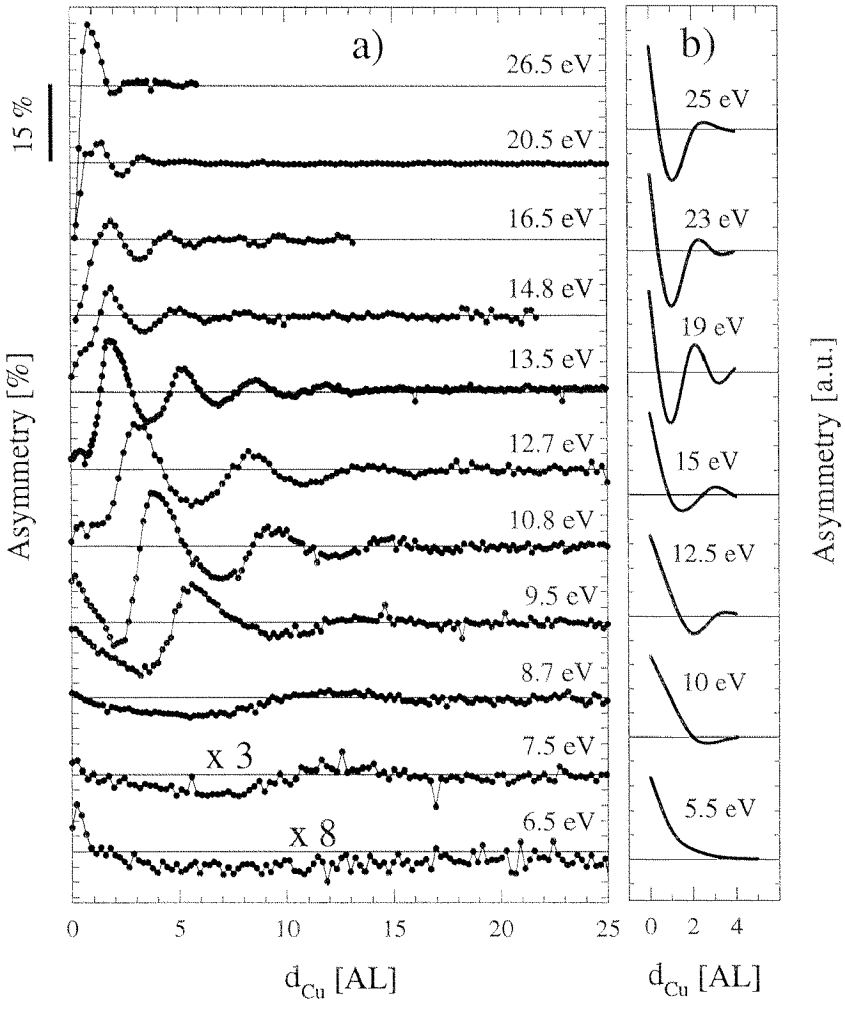

Figure 3.3: *a) Set of experimental $A(d_{\mathrm{Cu}})$ curves taken for different energies, the underlying Co film being $\approx$ 5 AL thick. b) Calculated spin asymmetry [26] (normalized to its value at $d_{\mathrm{Cu}} = 0$). The calculations have been performed at integer numbers of d_{Cu}: shown is the spline interpolation. Both sets of curves show one single oscillatory component. It is evident by inspection that the period of the oscillation grows when a lower energy limit is approached.*

However, the divergence of the period now appears at higher energies of $E_0 \approx 10.9$ eV. This is consistent with the picture of the unoccupied bands in Co being effectively shifted with respect to Cu by $\approx 1-2$ eV towards higher values [10, 31].

3.4 Connection to IXC

As an important experimental application of spin dependent electron interferometry we determine the energy dependence of the oscillation period $\Lambda(E)$ and show that the experimental $\Lambda(E)$ diverges when E approaches the band edge at the Brillouin zone boundary. According to Bruno [32] and Stiles [33], $A(d_{\mathrm{Cu}})$ is the origin of interlayer exchange coupling (IXC). Thus, the results of this chapter demonstrate some aspects of IXC which have not yet been detected experimentally, like the energy dependence of the IXC oscillation period and its divergence when a Brillouin zone boundary is approached [34, 35].

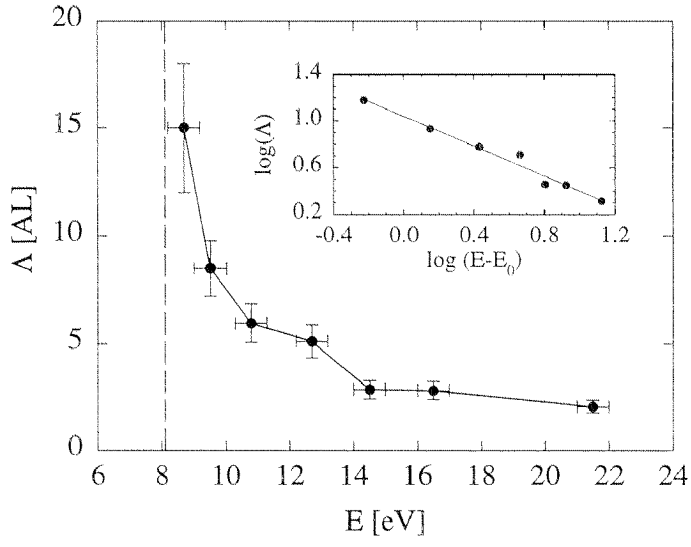

Figure 3.4: *Experimental values of Λ as a function of the energy for Cu/Co/Cu(100). The uncertainty of the energy is the width of the elastic peak in the energy spectrum of the specularly reflected electrons. The data in this figure suggests a lower energy limit E_0 at ≈ 8.1 eV. Inset: the same data plotted in a log-log scale, demonstrating the power law dependence of the period on the energy. The best fit to the data is a straight line with slope -0.61.*

Considering that $A(d_{Cu})$ is the origin of interlayer exchange coupling (IXC) [32, 33], we might think of the present interferometer as an experimental simulation of this phenomenon. In standard IXC experiments, two magnetic films are magnetically coupled through a non-magnetic spacer acting as a resonator. Upon varying the spacer thickness, the coupling of the two films changes periodically between ferromagnetic and antiferromagnetic, the periods being determined by the extremal spanning vectors of the Fermi surface [32, 33]. Typically, there are many periods, corresponding to different parallel components of the extremal spanning vector [33]. With respect to standard IXC experiments, the present spin interferometer allows for the first time to select one single parallel momentum and to investigate the energy dependence of the coupling period, thus extending the understanding of coupling phenomena beyond the constraint $E = E_F$ (E_F: Fermi energy). The

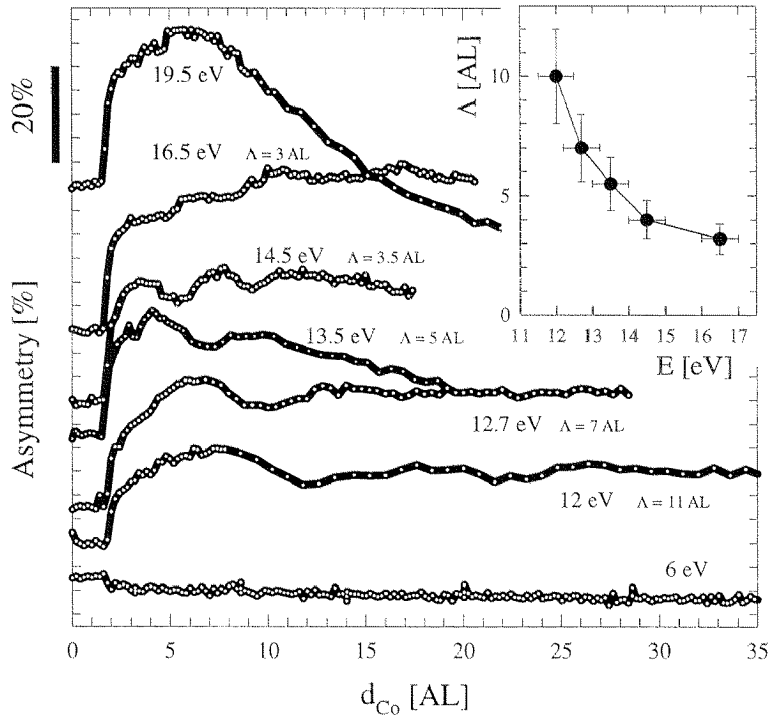

Figure 3.5: *A as a function of the Co film thickness for different electron energies. (The plots are shifted vertical. A_{ex} is zero at d_{Co}=0.) Inset: The period Λ as a function of the electron energy. The data in this figure suggest a lower energy limit E_0 at ≈ 10.9 eV. The accuracy of the data is not enough for a reliable critical exponent determination.*

results presented in Figs. 3.1–3.4 demonstrate the following:

i) Restricting the parallel momentum to one single component produces the selection of one single period, see Fig. 3.3, in agreement with our understanding of IXC [33].

ii) The oscillation in $R_{\mathrm{up}}(d_{\mathrm{Cu}})$ and $R_{\mathrm{down}}(d_{\mathrm{Cu}})$ has the same period, in agreement with IXC-models [33].

iii) The coupling period might be very short but can become very large if the energy approaches a band edge, see Fig. 3.4. This was realized in the earlier days of IXC [34, 35] but never systematically tested. In fact, studying the energy dependence of the period in standard IXC experiments requires resorting to a spacer with varying Fermi surface. The present experiment allows the spacer material to be kept the same while the energy is varied, thus eliminating uncertainties such as varying film morphology.

iv) Some models of IXC assume a free electron like character for the carrier of IXC within the spacer [32, 33], while other authors stress the importance of QWS [32, 33, 36, 37]. In our experiment, both models give rise to $\Lambda(E) \propto (E - E_{Bz})^{\beta}$. Within the QWS model, $\beta = -1/2$, see $\Lambda^{\mathrm{LP}}(E)$. Free electrons, *if sampled at integer number of layers* [35, 37], have a singularity as well, albeit with $\beta = -1$. The experimental value of β, see Fig. 3.4, indicates that a QWS model is more suitable to describe electrons within the Cu spacer.

3.5 Reflected Intensity for Co on Cu(100)

In this section the electron beam is *not* polarized. In the energy range from 6 to 13 eV we see monolayer oscillations in the electron reflectivity (Fig. 3.6 a,b). Because the growth of cobalt on copper is almost layer by layer [4], we explain these oscillations with the change in surface smoothness when the growth of each monolayer is completed — similarly to the one mono-layer oscillations observed in RHEED [16, 38]. If we subtract the fitted oscillations we see a depression over the first two atomic layers (Fig. 3.6 d). As the sample starts to be ferromagnetic at 1.6 AL (see Fig. 3.5), we attribute this feature to the onset of ferromagnetic order. Whether this is due to e.g. magnetostriction, we do not know yet.

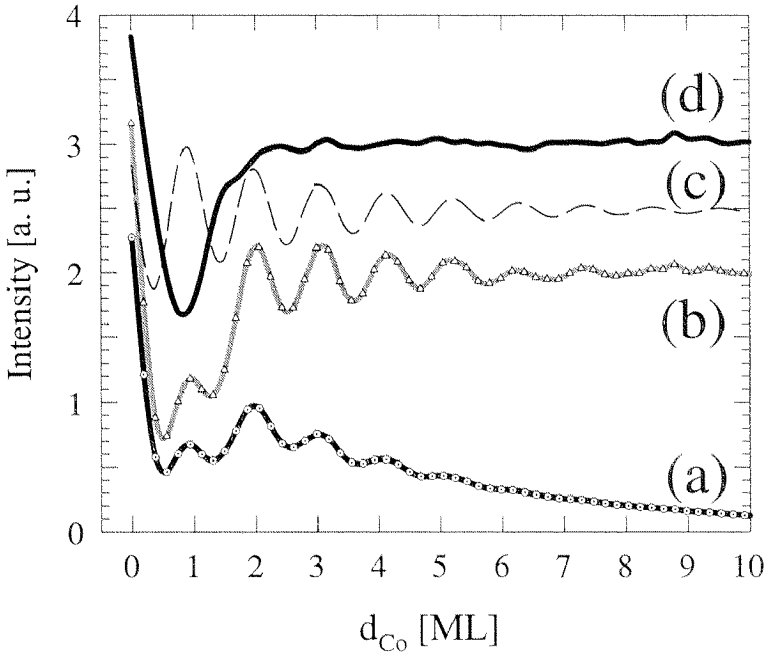

Figure 3.6: *LEED Intensity of Co on Cu(100), the electron energy is 12.7 eV: a) measured data (vertical scale in million counts), the asymptotic decay is caused by the dying electron source, b) intensity divided by the exponential decay, c) fitted oscillations, d) fitted oscillations subtracted.*

Chapter 4

Interlayer Exchange Coupling

Magnetic films separated by a non-magnetic metallic spacer can couple magnetically through the non-magnetic spacer layer [39, 40] and the coupling oscillates typically between ferromagnetic and antiferromagnetic. Since the discovery of this effect, the coupling has been subject of much experimental and theoretical interest. Many different systems were investigated (for an overview see e.g. reviews by Stiles [33] and Bruno [32]). To give an idea about the mechanism I will sketch the theory, following Stiles [33] and Bruno [32].

In a metal (in our experiments a copper single crystal) all electron states up to the Fermi energy E_F are filled. We introduce two magnetic films A and B (cobalt) inside the crystal (the distance between them is D). Now the electrons see two potential barriers. Some of the electrons in the spacer are reflected at these barriers. The phase shift for a complete round trip is

$$\Delta\phi = 2k_\perp D + \phi_A + \phi_B$$

where $\phi_{A,B}$ are the (quantum) phase shifts due to a reflection. If $\Delta\phi = 2n\pi$ (n an integer) the interferences are constructive, if $\Delta\phi = (2n+1)\pi$ the interferences are destructive. This affects the density of states in the spacer. The change in total ground state energy due to these reflections is the integral over all electrons within the spacer:

$$\Delta E(D) = \int_{-\infty}^{E_F} dE(E - E_\mathrm{F})\Delta n(E, D) \tag{4.1}$$

where $\Delta n(E, D)$ is the change in the density of states of an electron with energy E. As our films are magnetic, the potential barriers are

different for electrons with spin parallel or antiparallel to the magnetization. This leeds to a difference in the total energy for both Co films magnetized parallel or antiparallel. This difference is responsible for the coupling. In Eq. (4.1) we have to integrate over all states in the first Brillouin zone. The integrand contains oscillating components with different periods, depending on the energy. Due to cancellation, just those periods corresponding to extremal Fermi-surface spanning vectors survive [41]. This leeds to the asymptotic (large D) coupling energy per unit area for spherical [42] Fermi surface of

$$\xi = \frac{E_{\mathrm{F}} - E_{\mathrm{AF}}}{A} =$$

$$-\frac{\hbar}{2\pi^2}\left[\frac{k_F v_F}{4}\right]\left(|R_{\mathrm{up}}|^2 + |R_{\mathrm{down}}|^2 - 2|R_{\mathrm{up}}R_{\mathrm{down}}|\right)\frac{\sin(2k_F D + \phi)}{D^2} \tag{4.2}$$

$R_{\mathrm{up(down)}}$ is the reflection amplitude for an electron with spin parallel (antiparallel) to the magnetization. We have oscillations with $\Lambda = \pi/k_F$ and a decay like $1/D^2$.

To perform coupling experiments, we have deposited a Cu wedge between the Co films. This wedge acts as a spacer with variable thickness (Fig. 4.1). To determine the coupling energy we used MOKE, which measures the strength of the antiferromagnetic coupling by recording directly magnetic field required to obtain parallel alignment of both Co films (see Fig. 1.2c).

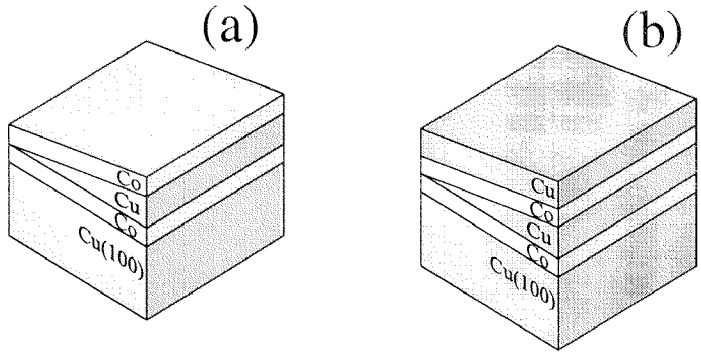

Figure 4.1: *Wedge Structures: a) Co/Cu/Co/Cu(100), b) additional copper cap layer. The lateral size of our structures is about 4 mm. The slope of the wedge is 10 AL/mm and the typical thickness for a Co film is 5 AL.*

4.1 Variable Spacer-Thickness

In a Co/Cu(100) tri-layer system two different periods $\lambda = 2.5$ AL and $\Lambda = 5.5$ AL can be observed. The relative strength of the oscillations associated with the two periods depends on the temperature at which the Cu spacer was grown and the measurement was performed.

i) Growth and measurements at room temperature: Λ is easy to identify [43], λ is rather weak (or not visible at all). The roughness of the upper Co/Cu interface disturbs the small period.

ii) Grown at measured at lower temperature (170 K): The small period dominates the spectra. The thickness fluctuations are smaller and the experimental data are closer to the theoretical expectations [6, 44].

4.1.1 Temperature Dependence

Systems grown at 170 K and measured at different temperatures show a temperature dependence of the exchange coupling strength [3]. The temperature dependence is stronger then expected by theory [32, 41] and only partially reversible. The presence of two periods Λ and λ makes the interpretation difficult.

How is the temperature dependence for systems deposited at room temperature? After depositing the structure at 300 K we performed a series of measurements repeatedly scanning the temperature between 300 K and 50 K. The coupling is shown in Fig. 4.2 (a and c at 300 K, b and d at 50 K). All curves are dominated by the large period (Λ=5.5 ML). The changes at spacer thickness between 13 AL and 20 AL are not reversible. This suggest a structural change. But for spacer thickness larger than 20 AL the plots corresponding to the same temperature are very similar.

What does theory predict? By assuming Fermi-Dirac statistics (may be there are additional contributions: Almeida *et al.* [45] proposed a model of spin wave interactions in magnetic multilayers) Bruno [32] calculates the temperature dependence of the coupling strength to be

$$t_\alpha(D,T) = \frac{c_\alpha DT}{\sinh(c_\alpha DT)} \tag{4.3}$$

with

$$c_\alpha = \frac{2\pi k_B}{\hbar v_F^\alpha}$$

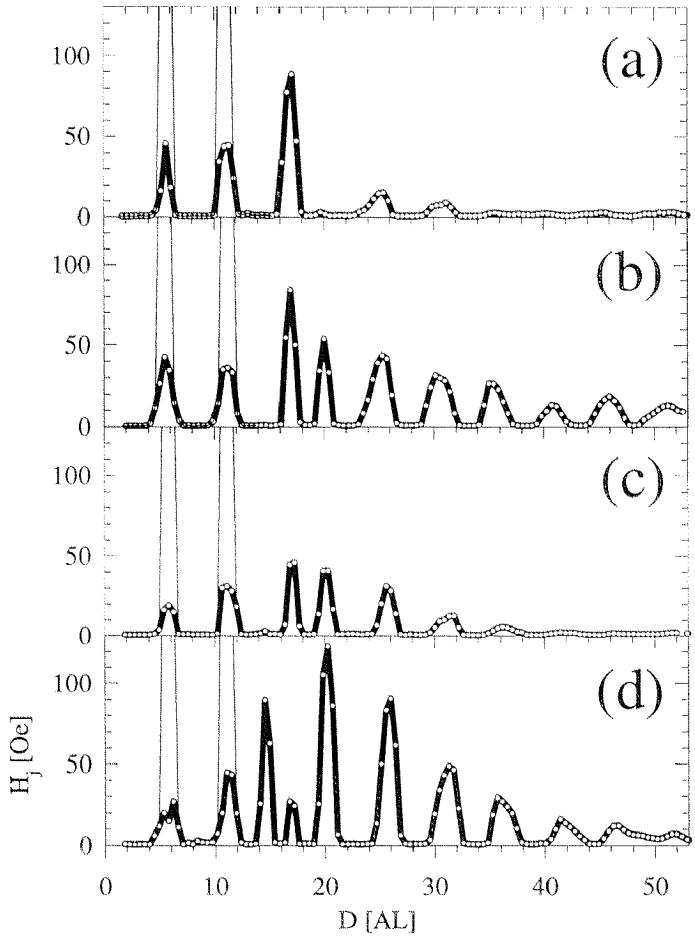

Figure 4.2: *Coupling field versus spacer thickness, wedge structure like Fig. 4.1a, both Co films are 7 AL thick, all films were evaporated at room temperature: a) measured at room temperature, b) cooled down to 50 K and measured again, c) back at room temperature, d) cooled a second time at 50 K. For the first two peaks (5.5 AL and 11 AL) the field was not strong enough to saturate the magnetization.*

where α labels the spanning vector, v_F^α its Fermi velocity, k_B the Boltzmann constant and D the spacer thickness. Our length unit is the spacing between atomic planes (AL). Drchal *et al.* [46] compute the temperature dependence of IXC by employing an *ab initio* approach. They found good agreement by setting $c_\lambda = 1.9 \cdot 10^{-4}$ $\mathrm{K^{-1}AL^{-1}}$ (short period) and $c_\Lambda = 2.75 \cdot 10^{-4}$ $\mathrm{K^{-1}AL^{-1}}$ (long period).

We compare this theory with the experiment (Fig. 4.2). The theoretically expected temperature dependence is in average about two

times smaller then in the experiment (Table 4.1). For larger spacer thickness it is even smaller. To get the experimental temperature dependence $c_{\Lambda,\mathrm{exp}}$ has to be $3.7 \cdot 10^{-4}$ $\mathrm{K}^{-1}\mathrm{AL}^{-1}$.

Peak at $N \approx$	Experiment	Theory
31 AL	≈ 3.9	2.4
36 AL	≈ 6.7	3.1
41 AL	≈ 10	4.1

Table 4.1: *$\xi(N, 50\ K)/\xi(N, 300\ K)$. Relative change in exchange energy at different temperatures 50 K and 300 K. The experimental values are derived from Fig. 4.2. The theoretical values are calculated with c_Λ=2.75 $\cdot 10^{-4}$ $K^{-1}AL^{-1}$*

4.2 Variable Cu Cap Layer

De Vries *et al.* [47] investigated IXC of the Co/Cu system with a variable cap layer. They used a double wedge structure: the first wedge was used as a spacer and the second one (turned by 90°) as a cap layer. To protect the structure, they deposited an additional gold film on top. They found an oscillatory change in some antiferromagnetic coupling peaks as a function of the cap layer thickness. The period is about 5 AL. Bounouh *et al.* [48] did theoretical and experimental studies about Co/Au tri-layers. In the experiment the oscillations were very weak.

We worked in the following way: after growing both Co films and the spacer wedge between them, we performed simultaneous growth of the cap layer and scans with MOKE. Fig. 4.3 maps the coupling as a function of the spacer thickness D and the cap layer thickness T. The contour plot is derived from 44 scans at different cap layer thicknesses. We clearly observe changes in the strength and the **sign** of the coupling due to the cap layer.

In Fig. 4.4 the corresponding Fourier power spectrum is shown. Both the long and short periods are visible. In addition, they occur in two different directions of the Fourier space.

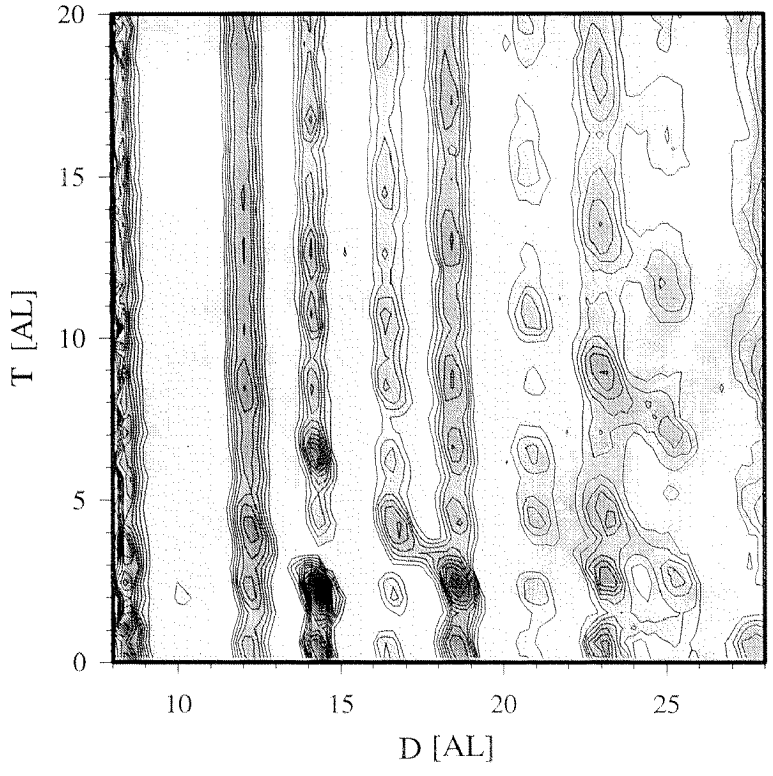

Figure 4.3: *Shift field of Cu/Co/Cu/Co/Cu(100) as a function of both Cu film thicknesses. Horizontal: spacer thickness D, vertical: cap layer thickness T. White: ferromagnetic, dark: antiferromagnetic regions. Contour plot with 3 Oe per line. Measured at room temperature. The Co films are about 7 AL thick.*

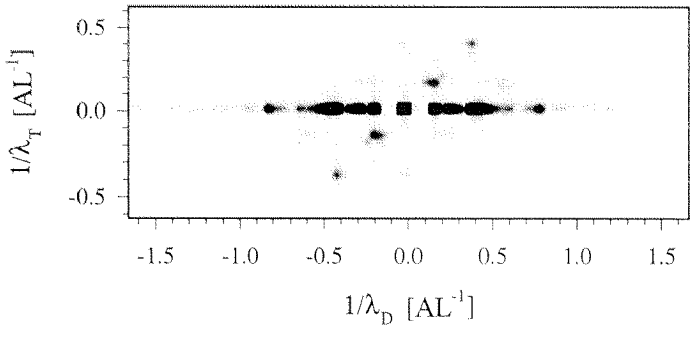

Figure 4.4: *Fourier spectra of Fig. 4.3.*

The strongest peaks are along the horizontal axis (in Fig. 4.3 out of range), and indicate oscillations as a function of D at fixed cap thickness T

$$A\cos\left(\frac{2\pi D}{\Lambda}+\phi_1\right)+a\cos\left(\frac{2\pi D}{\lambda}+\phi_2\right). \tag{4.4}$$

There are weaker peaks on one diagonal

$$B\cos\left(\frac{2\pi(D+T)}{\Lambda}+\phi_3\right)+b\cos\left(\frac{2\pi(D+T)}{\lambda}+\phi_4\right) \tag{4.5}$$

and a very week peak on the ordinate with the small period: $\cos(\frac{2\pi T}{\lambda}+\phi_1)$.

The observed periods are Λ=5.5 AL and λ=2.5 AL.

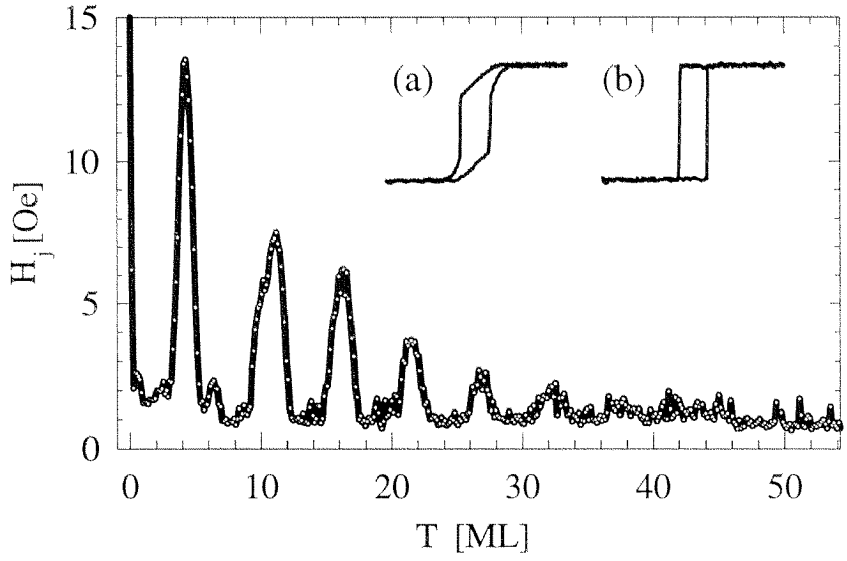

Figure 4.5: *Interlayer exchange coupling of Cu/Co(3 AL)/Cu(19 AL)/ Co(5 AL)/Cu(100) as a function of the top Cu film thickness. Films grown at room temperature. The cap layer changes the sign of the coupling. a) Hysteresis loops at 11 AL: antiferromagnetic and b) at 13 AL: ferromagnetic, for both loops H_{max} =50 Oe.*

One interesting feature is not clearly visible from the contour plots of Fig. 4.3, namely the switch of sign. For the purpose of optimally detecting this feature, we have kept the spacer thickness constant and perform MOKE experiments during the growth of the cap layer (this

corresponds to a vertical line scan in Fig. 4.3. In Fig. 4.5 we plot the result for $D = 19$ AL. The cap layer changes the coupling between ferromagnetic and antiferromagnetic with the period $\Lambda = 5.5$ AL.

Theory predicts that oscillations decay like $1/(D + L_2 + T)^2$ for IXC oscillations at 0 K [32, 49, 50]. To take into consideration finite temperatures the factor $t_\Lambda(D,T) = c_\Lambda DT/\sinh(c_\Lambda DT)$ (Eq. 4.3) has to be multiplied. Fig. 4.6 shows a IXC measurement at room temperature. The dotted line is an envelopes for $T = 0$ K. The dashed and solid lines are envelopes for $T = 300$ K, calculated with different coefficients c_Λ: the theoretically expected coefficient is [46] $c_\Lambda = 2.75 \cdot 10^{-4}$ $K^{-1}AL^{-1}$ (dashed) and that which best fits the experimental data is ($c_\Lambda = 1.9 \cdot 10^{-4}$ $K^{-1}AL^{-1}$).

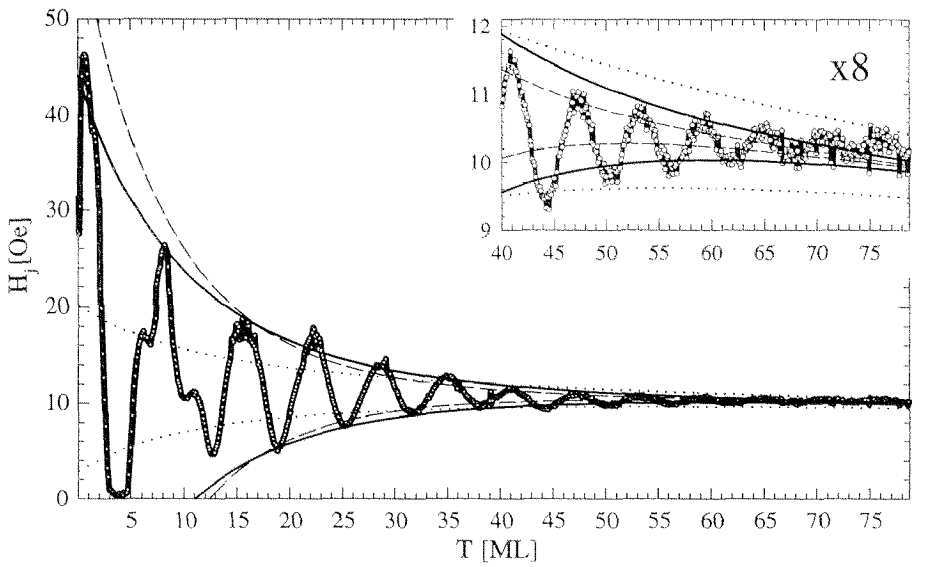

Figure 4.6: *Shift field of Cu/Co(5 AL)/Cu(20.5 AL)/Co(3.5 AL)/Cu(100) as a function of the top Cu film thickness. All films grown at room temperature. Dotted line* $\propto 1/(L_2 + D + T)^2$, *dashed and solid:* $\propto (c_\Lambda DT)[\sinh(c_\Lambda DT)]^{-1}(L_2 + D + T)^{-2}$ *with* $c_{\Lambda,th}$ $=2.75 \cdot 10^{-4}$ $K^{-1}AL^{-1}$ *[46] (dashed) and* $c_{\Lambda,exp}$$=1.8 \cdot 10^{-4}$ $K^{-1}AL^{-1}$ *(solid).*

As mentioned in chapter 2 (p. 10) our Cu(100) crystal has a miscut of 0.7°. This miscut induces a two-fold magnetic anisotropy (in addition to the four-fold crystal anisotropy). So far we have applied our external field along the easy magnetization axis (the direction which is preferred by spins). Measuring *perpendicular to the easy axis* has the advantages that even without antiferromagnetic coupling the loops

are shifted [5, 6, 51] (see also Fig. A.1). There is a background in our curves. On this background it is easier to see the oscillations due to IXC. The disadvantage is that the measured shift is caused by a mixture of anisotropy and coupling. However, the anisotropy changes of a Co film induced by a Cu film on top are small [3, 52]. In Fig. 4.7 we show a plot of the shift field taken in the "perpendicular-to-easy-axis-mode": The Co-Cu-Co structure feels the interface between Cu cap layer and

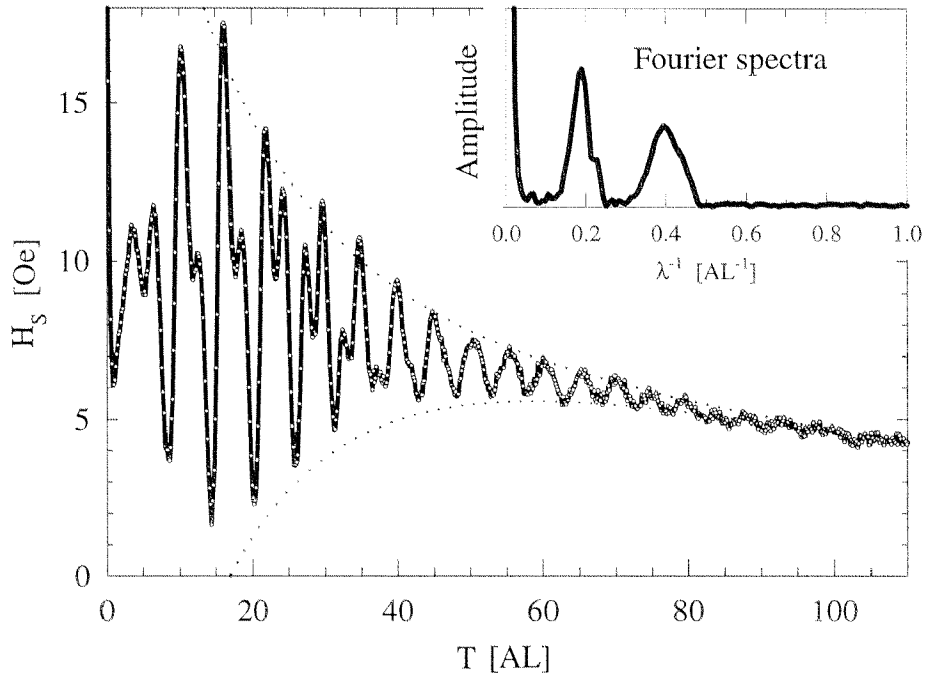

Figure 4.7: *Shift field of Cu/Co(6 AL)/Cu(26 AL)/Co(6 AL)/Cu(100) as a function of the top Cu film thickness, measured perpendicular to the easy axis. The first Co film was grown at room temperature, the other films were deposited on cooled sample (170 K until starting growth of cap layer, the temperature was drifting linearly up to 230 K). Dotted: difference between both lines* $\propto (c_\Lambda DT)[\sinh(c_\Lambda DT)]^{-1}(L_2+D+T)^{-2}$ c_Λ=$1.8 \cdot 10^{-4}$ $K^{-1}AL^{-1}$.

the vacuum at distances as far as 100 AL! The Fourier power spectrum displays both periods Λ and λ, the shorter one decaying faster than the longer one. (A similar measurement at room temperature is given in the Appendix A, Fig. A.1.)

4.3 Variable Co Film Thickness

So far we investigated always structures with constant Co film thickness. Does the thickness of the magnetic films affect the IXC? Okuno *et al.* [53, 54] investigated the system Fe/Cr(100). They found oscillatory behaviors as a function of the Fe layer thickness. Bloemen *et al.* [55] studied the first two antiferromagnetic peaks of the Co/Cu(100) system. They found 6–7 Å ($\approx$ 3.5 AL), but with rather poor experimental data.

We grow a structure like Fig. 4.1a. When we growth the second Co film we scan the sample with MOKE. This allows us to map the IXC as a function of both the spacer- and top Co film thickness (Fig. 4.8). Beside the expected oscillations as a function of the spacer thickness we see also oscillations as a function of the Co thickness. The period is about 2 ML. For thin spacer layer thickness the changes are dramatic.

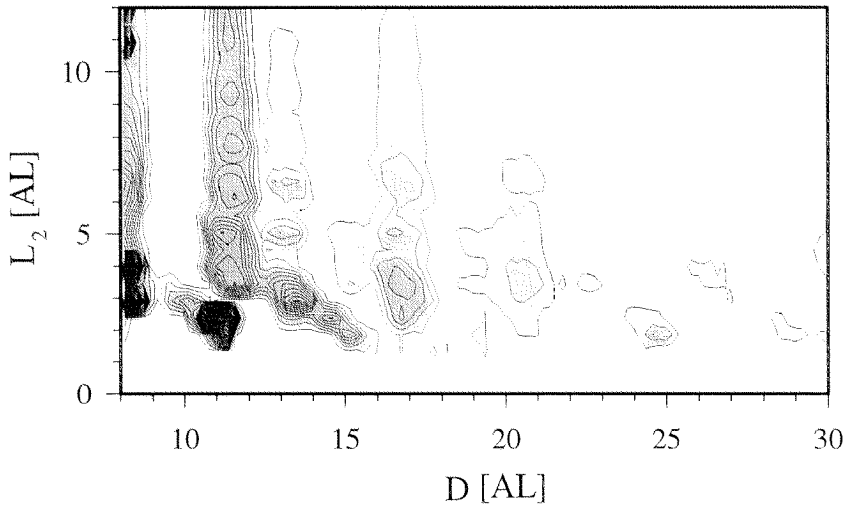

Figure 4.8: *Shift field of Co/Cu/Co(7 AL)/Cu(100) as a function of the Co and Cu film thicknesses. Contour plot with 8 Oe per line.*

More details of the dependence of IXC on the Co thickness are obtained from experiments where only the Co thickness is varied. In Fig. 4.9 (same measurement as in Fig. A.1) the spacer layer is 21 AL thick. In Fig. 4.9c the coupling is oscillating as a function of L_2 with a period of 2 AL. The thickness of the Co is cross checked with with the monolayer oscillations in Fig. 4.9a [16].

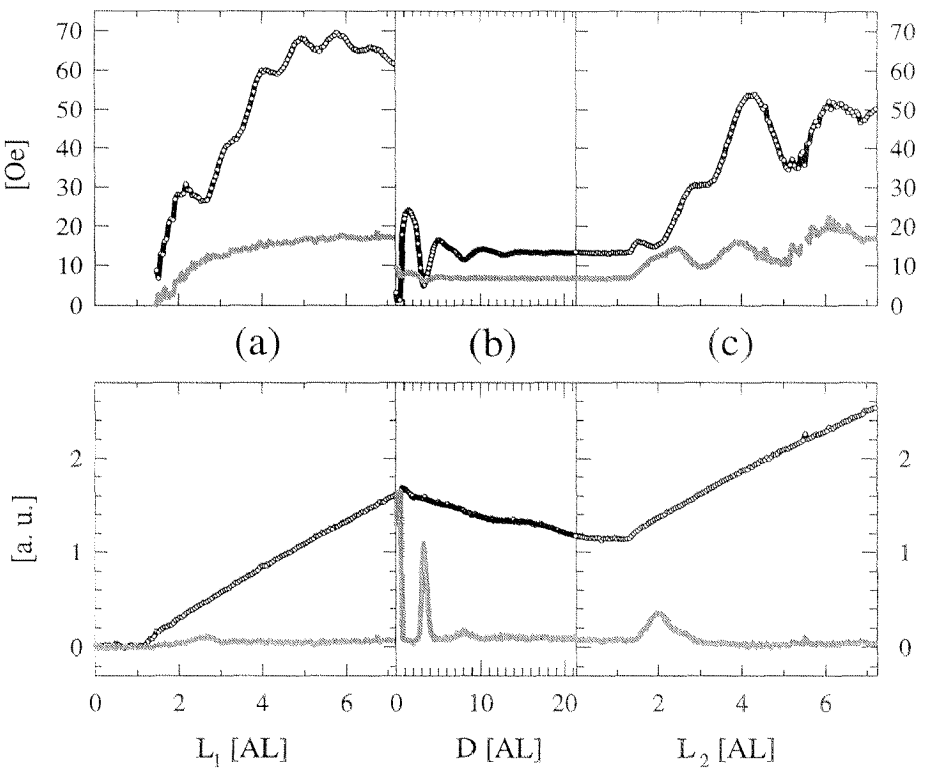

Figure 4.9: *Upper part: shift field (black, white points), coercitive field (gray). Lower part: saturation magnetization (black, white points), remanence (gray). Measured during growth at room temperature. a) First Co layer: monolayer oscillations b) Cu layer [6], c) second Co layer: oscillations with λ =2 AL and weak monolayer oscillations at the begin.*

4.4 Comparison with Theory

Among the many numerical and analytical calculations of IXC [32, 33, 56, 57, 58], we concentrate on the model proposed by Bruno.

4.4.1 Quantum Well Model

Bruno [59] wrote for weak confinement the following formula:

$$E_{\mathrm{F}} - E_{\mathrm{AF}} \approx$$

$$\frac{\hbar^2}{8\pi^2 m}\,\mathrm{Im}\left\{ {r_\infty}^2 e^{2ik_F D}\left(\frac{1}{\left(\frac{D}{k_F}\right)^2} - \frac{e^{2ik_F^{\downarrow}L_1}}{\left(\frac{D}{k_F}+\frac{L_1}{k_F^{\downarrow}}\right)^2} - \frac{e^{2ik_F^{\downarrow}L_2}}{\left(\frac{D}{k_F}+\frac{L_2}{k_F^{\downarrow}}\right)^2} + \frac{e^{2ik_F^{\downarrow}(L_1+L_2)}}{\left(\frac{D}{k_F}+\frac{L_1+L_2}{k_F^{\downarrow}}\right)^2}\right)\right.$$

$$-r_\infty r_v e^{2ik_F(D+T)}\left[\frac{e^{2ik_F L_2}}{\left(\frac{D+T+L_2}{k_F}\right)^2} - \frac{e^{2ik_F^{\downarrow}L_2}}{\left(\frac{D+T}{k_F}+\frac{L_2}{k_F^{\downarrow}}\right)^2}\right.$$

$$\left.\left. - \frac{e^{2ik_F L_2+2ik_F^{\downarrow}L_1}}{\left(\frac{D+T+L_2}{k_F}+\frac{L_1}{k_F^{\downarrow}}\right)^2} + \frac{e^{2ik_F^{\downarrow}(L_1+L_2)}}{\left(\frac{D+T}{k_F}+\frac{L_1+L_2}{k_F^{\downarrow}}\right)^2}\right]\right\} \tag{4.6}$$

where L_1, D, L_2 and T are the thicknesses of layers, deposited in this order. ${r_\infty}^2$ and r_v are the complex reflectivities due to a semi infinite steps with height V (magnetic half space) and W (vacuum) respectively. $|r_v| = 1$, because the vacuum barrier is higher then the particle energy. The meaning of each summand is visualized in Fig. 4.10. We compare this formula with the experimental result.

i) On page p. 28 the terms observed in the experimental spectra Fig. 4.4 are listed. The term (4.4) corresponds to the the upper line in Eq. (4.6). The term in square braces in Eq. (4.6) does not oscillate for fixed $L_{1,2}$. The term just in front of it is the only one oscillating as a function of T. The analog to term (4.5).

ii) The term in square braces in Eq. (4.6) falls off like $\approx 1/(D+T+L)^2$ (if L is small compared to $D+T$ the additional L in the dominator of some terms does not affect the sum much, further k_F is not far away from $k_F^{\downarrow}$). In Fig. 4.6 (p. 29) the dotted line is proportional to $1/(D+T+L)^2$.

iii) The oscillations as a function of one Co layer thickness (period 2 AL) could not be explained. In Eq. (4.6) all terms oscillating with L_2 do also oscillate as a function of D with about the same period. The qualitative agreement is good when the Cu film thicknesses are varied.

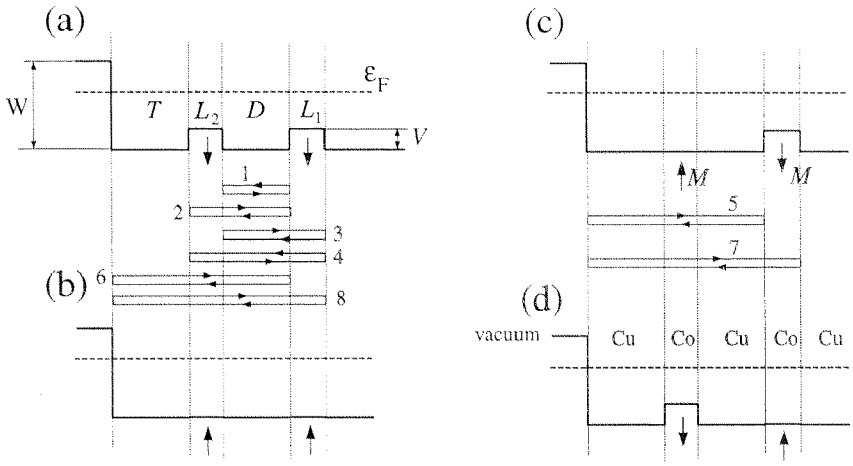

Figure 4.10: *IXC model: If the magnetization is parallel to their spin the electrons see a potential V, otherwise the potential vanishes. Four possible configurations: a), b) ferromagnetic coupling, c), d) antiferromagnetic coupling. Only a) and c) are relevant. The IXC energy is the difference of these configurations. Each term in Eq. (4.6) corresponds to a closed path, connecting interfaces of both magnetic films. The interferences change the density of states and this affects the energy. The numbers in the figure indicate the position. Terms with more then two reflections (leading to shorter oscillation periods) are neglected in Eq. (4.6).*

But because $|r_\infty|$ is small compared to $|r_v|$, the terms in line two and three dominate for $D > T$ (see contour plot in [59]). The experiment shows just the opposite.

4.4.2 Ruderman-Kittel-Kasuya-Yosida Model

An other approach to calculate the interlayer exchange coupling is the Ruderman-Kittel-Kasuya-Yosida (RKKY) model. Baltensperger and Helman [49, 50] found for the interlayer exchange coupling of *two infinitely thin magnetic planes* in a metal half space the following formula:

$$\xi_1 = \frac{-\beta\beta' \mathbf{I}\cdot\mathbf{I}' k_F^2 m}{(2\pi\hbar)^2} \{G(2k_F D) - 2G[2k_F(D+T)] + G[2k_F(D+2T)]\} \tag{4.7}$$

with

$$G(v) = \frac{\pi}{4} - \frac{\mathrm{Si}(v)}{2} - \frac{\sin(v) + v\cos(v)}{2v^2} \approx \frac{\sin(v)}{v^2}$$

where D is the spacer and T is the cap layer thickness. k_F has to be equal (π/Λ) or (π/λ). $\mathbf{I}$ and $\mathbf{I}'$ are the magnetization directions.

We try to relate the terms in 4.7 to the term recorded in the experiments (Fig. 4.4, p. 27):

- The first term in Eq. (4.7) corresponds to the term (4.4).
- The second to the term (4.5).
- The last one is not observed in the experimental spectra (no point at $(\lambda_D, \lambda_T) = (0.2, 0.4)$), but this is indeed the weakest term in Eq. (4.7).
- The decay $\propto 1/(D+T)^2$ of Eq. (4.7) is similar to the decay in Fig. 4.6.

In Fig. 4.11 we show a contour plot of Eq. (4.7) with two different k_F. The weight of the two periods was chosen to fit the experimental results. The Fourier spectrum Fig. 4.12 reproduces well the experimental one.

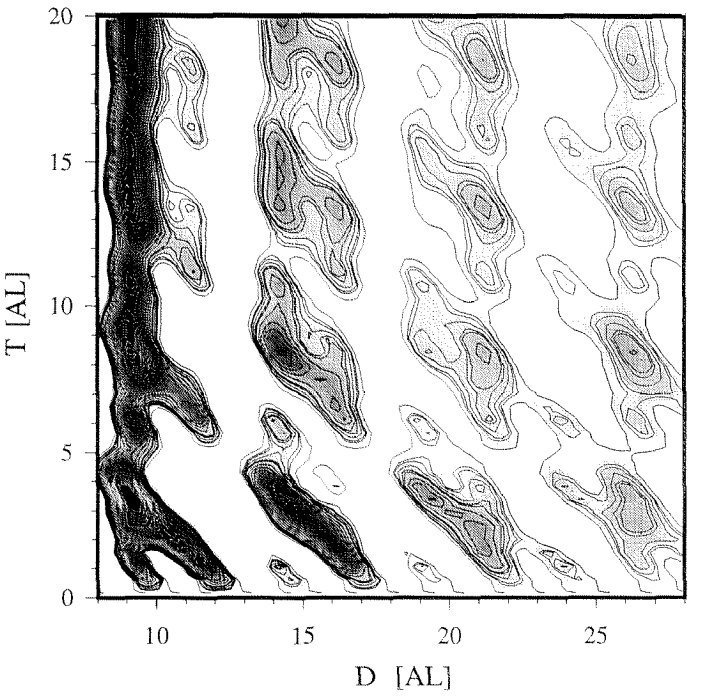

Figure 4.11: *Contour plot of Eq. 4.7 with two periods,* $c\,\xi_1(L,T,k_F = \frac{\pi}{2.5\ AL}) + C\,\xi_1(L,T,k_F = \frac{\pi}{5.5\ AL})$ *with (c=3, C=1).*

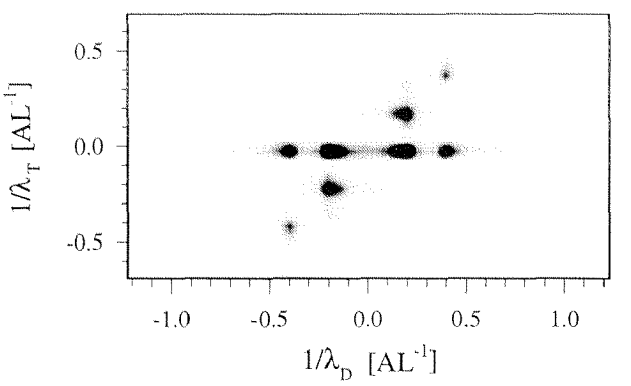

Figure 4.12: *Fourier spectra of Fig. 4.11. The same spots as in Fig. 4.4, the spot corresponding to the third term in Eq. 4.7 is not visible in this scale.*

Appendix A

MOKE Oscillations Summary

Fig.A.1 is a summary of some oscillatory effects observed in thin magnetic films. MOKE and growth were simultaneously performed.

First Co film:
Because the measurement in Fig.A.1 was performed perpendicular to the easy anisotropy axis, the hysteresis loops were shifted (almost no remanence). Mono-layer oscillations are visible in the shift field. [16].

First Cu film:
Shortly after starting the growth of a copper layer the shift field decreases dramatically [52] and starts oscillating with a period of about 5.5 AL [6].

Second Co film:
The second cobalt film is coupling with the first one. We observe two peaks (see section 4.3).

Second Cu film:
The coupling field is oscillating as described in section 4.2. There are two periods (λ = 2.5 AL and Λ = 5.5 AL): the short one is rather weak, but the long period is visible for about 70 AL. In the coercitive field we can identify the short period very clearly.

1st and 2nd Cu film:
We find an other kind of oscillation with $\Lambda_{sat} \approx 15$ AL in the saturation magnetization (see [3] and references therein).

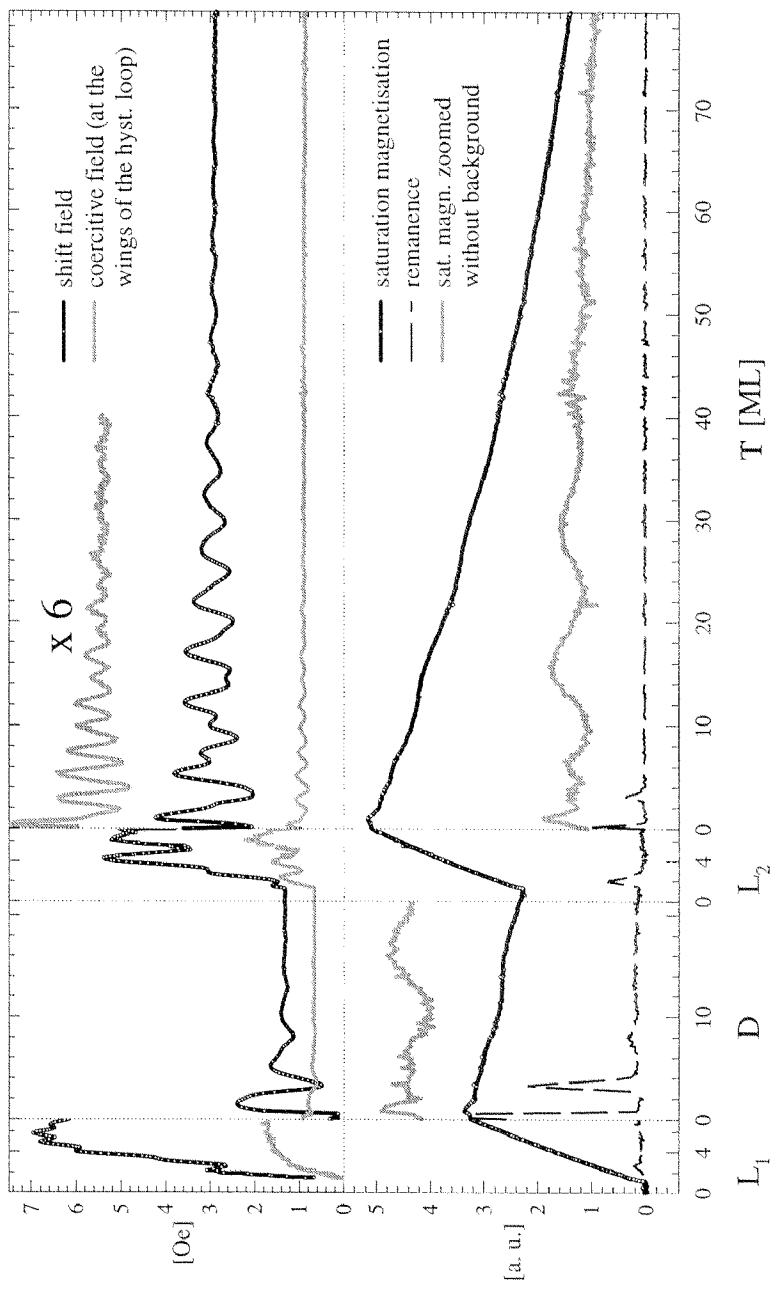

Figure A.1: *MOKE measurements performed at room temperature during growth for Cu/Co/Cu/Co/Cu(100). Applied field perpendicular to the easy axis.*

Appendix B

Asymmetry Due to a Step

To explain the origin of the exchange asymmetry in terms of the exchange energy v we consider a semi infinite quantum well. Electrons with spin parallel (anti-parallel) see a potential step $U+v(U-v)$. The reflection probabilities (see quantum mechanics text books) for both spin directions are

$$R_{\substack{\text{up}\\\text{down}}} = \frac{\left(\sqrt{U} - \sqrt{U \pm v - V}\right)^2}{\left(\sqrt{U} + \sqrt{U \pm v - V}\right)^2}.$$

This gives the spin asymmetry

$$A \equiv \frac{R_{\text{up}} - R_{\text{down}}}{R_{\text{up}} + R_{\text{down}}}$$

$$= \frac{2\sqrt{U}\left(\sqrt{U-v-V}\,(2U+v-V) + \sqrt{U+v-V}\,(-2U+v+V)\right)}{-v^2 - 4U\sqrt{U-v-V}\sqrt{U+v-V} + (-2U+V)^2}.$$

For $v \ll V$ we have

$$A \approx -\sqrt{\frac{U}{U-V}} \cdot \frac{2v}{V}$$

and if also $U \gg V$

$$A \approx -\frac{2v}{V} - \frac{v}{U}.$$

(The reflection probabilities for $v = 0$ and $U \gg V$: $\quad R \approx \frac{V^2}{16\,U^2}$).

Appendix C

RKKY, Two Magnetic Slabs

Baltensperger [50] derived also a formula for *two magnetic slabs* in a semi infinite non-magnetic metal:

$$\begin{aligned}\xi_2 = \frac{-\alpha\alpha' \mathbf{I}\cdot\mathbf{I}' k_F^2 m}{(2\pi\hbar)^2} \Big\{ & \Big. -G_2[2k_F D] \\ & +G_2[2k_F\,(D+L_1)] \\ & +G_2[2k_F\,(D+L_2)] \\ & \Big. -G_2[2k_F\,(D+L_1+L_2)] \Big\}\star \\ & \Big. +G_2[2k_F\,(D+2T+L_2)] \\ & -G_2[2k_F\,(D+2T+2L_2)] \\ & -G_2[2k_F\,(D+2T+L_1+L_2)] \\ & \Big. +G_2[2k_F\,(D+2T+L_1+2L_2)] \Big\}\dagger \\ & -4k_F L_2\Big(G_1[2k_F\,(D+T+L_1+L_2)] \\ & \quad -G_1[2k_F(D+T+L_2)]\Big)\Big\}\ddagger\end{aligned} \tag{C.1}$$

were

$$G_1(v) = \left(\frac{-\pi}{4} + \frac{\mathrm{Si}(v)}{2}\right) v + \frac{\sin(v) + v\cos(v)}{2\,v} \approx \frac{\cos(v)}{v^2}$$

and

$$G_2(v) = \left(\frac{\pi}{4} - \frac{\mathrm{Si}(v)}{2}\right)\left(1 + \frac{v^2}{2}\right) - \frac{(\sin(v) + v\cos(v))}{4} \approx -\frac{\sin(v)}{v^2}.$$

$\mathbf{I}$ and $\mathbf{I}'$ are the magnetization directions. α is the coupling constant with dimension energy x length. D is the spacer T the cap layer

thickness. L_1 is the thickness of the Co film who was evaporated first. k_F has to be equal (π/Λ) or (π/λ).

The lines marked with $\star$, † and ‡ correspond to the three terms in Eq. 4.7. The terms $\star$, ‡ and the decay for large T fit with the experimental data, the term † do not (but † is small, it was neglected in Eq. (4.6)). If we choose realistic Co film thicknesses the term ‡ dominates.

Bibliography

[1] H.C. Back, *Transitions and anisotropies in of ultra thin magnetic films*, Ph.D. Thesis, ETH Zürich, No. 11245 (1995), and references therein.

[2] U. Ramsperger, *Structural and magnetic investigations of ultrathin microstructures*, Ph.D. Thesis, ETH Zürich, No. 12092 (1997).

[3] Ch. Würsch, *Structural- and quantum-induced magnetic oscillations in ultra thin films* Ph.D. Thesis, ETH Zürich, No. 12091 (1997).

[4] U. Ramsperger, A. Vaterlaus, P. Pfaffli, U. Maier, D. Pescia, *Growth of Co on a stepped and on a flat Cu(001) surface*, Phys. Rev. B **53**, 8001–6 (1996).

[5] W. Weber, A. Bischof, R. Allenspach, C.H. Back, J. Fassbender, U. May, B. Schirmer, R.M. Jungblut, G. Guntherodt, B. Hillebrands, *Structural relaxation and magnetic anisotropy in Co/Cu(001) films*, Phys. Rev. B **54**, 4075–9 (1996).

[6] Ch. Würsch, C. Stamm, S. Egger, D. Pescia, W. Baltensperger, J.S. Helman, *Quantum oscillations in a confined electron gas*, Nature **389**, 937–9 (1997).

[7] E. Corcoran, *Diminishing dimensions*, Sci. Am. **263**, No. 5, 74 (1990).

[8] J.J. Paggel, T. Miller, T.-C. Chiang, *Quasiparticle lifetime in macroscopically uniform Ag/Fe(100) quantum wells*, Phys. Rev. Lett. **81**, 5632–5 (1998).

[9] M.A. Mueller, T. Miller, T.-C. Chiang, *Determination of the bulk band structure of Ag in Ag/Cu(111) quantum-well systems*, Phys. Rev. B **41**, 5214–20 (1990).

[10] J.E. Ortega, F.J. Himpsel, G.J. Mankey, R.F. Willis, *Quantum-well states and magnetic coupling between ferromagnets through a noble-metal layer*, Phys. Rev. B **47**, 1540–52 (1993).

[11] R.K. Kawakami, E. Rotenberg, H.J. Choi, E. Escorcia-Aparicio, M.O. Bowen, J.H. Wolfe, E. Arenholz, Z.D. Zhang, N.V. Smith, Z.Q. Qiu, *Quantum-well states in copper thin films*, Nature **398**, 132–4 (1999).

[12] M.F. Crommie, C.P. Lutz, D.M. Eigler, *Imaging standing waves in a two-dimensional electron gas*, Nature **363**, 524–7 (1993).

[13] Y. Hasegawa, P. Avouris, *Direct observation of standing wave formation at surface steps using scanning tunneling spectroscopy*, Phys. Rev. Lett. **71**, 1071–4 (1993).

[14] L. Bürgi, O. Jeandupeux, A. Hirstein, H. Brune, K. Kern, *Confinement of surface state electrons in Fabry-Perot resonators*, Phys. Rev. Lett. **81**, 5370–3 (1998).

[15] S. Egger, C.H. Back, J. Krewer, D. Pescia, *A spin selective electron interferometer*, Phys. Rev. Lett. **83**, 2833–6 (1999).

[16] W. Weber, C.H. Back, A. Bischof, Ch. Würsch, R. Allenspach, *Morphology-induced oscillations of the magnetic anisotropy in ultrathin Co films*, Phys. Rev. Lett. **76**, 1940–3 (1996).

[17] S.F. Alvarado, R. Feder, H. Hopster, F. Ciccacci, H. Pleyer, *Simultaneous probing of exchange and spin-orbit interaction in spin polarised low energy electron diffraction from magnetic surfaces*, Z. Phys. B **49**, 129–32 (1982).

[18] This component is damped when d_{Cu} is increased. The damping is due the electrons retaining their coherence only up to a finite depth because of inelastic scattering: if d_{Cu} becomes larger than this depth, interference between electrons reflected at the Cu/vacuum boundary and electrons reflected at the Cu/Co boundary is no longer possible

[19] T. Scheunemann, R. Feder, J. Henk, E. Bauer, T. Duden, H. Pinkvos, H. Poppa, K. Wurm, *Quantum well resonances in ferromagnetic Co films*, Solid State Comm. **104**, 787–92 (1997).

[20] P.D. Loly, J.B. Pendry, *Removing the limits to accurate band-structure determination by photoemission*, J. Phys. C **16**, 423–31 (1983).

[21] D. Park, *Introduction to the quantum theory*, McGraw Hill, New York, 1974, 2nd ed., pp. 96–102.

[22] H. Iwasaki, B.T. Jonker, R.L. Park, *Low-energy-electron transmission through epitaxial films: Cu(001) on Ni(001)*, Phys. Rev. B **32**, 643–54 (1985).

[23] R.C. Jaklevic, J. Lambe, M. Mikkor, W.C. Vassell, *Observation of electron standing waves in a crystalline box*, Phys. Rev. Lett. **26**, 88–92 (1971).

[24] K. Garrison, Y. Chang, P.D. Johnson, *Spin polarization of quantum well states in copper thin films deposited on a Co(001) substrate*, Phys. Rev. Lett. **71**, 2801–4 (1993).

[25] C. Carbone, E. Vescovo, O. Rader, W. Gudat, W. Eberhardt, *Exchange split quantum well states of a noble metal film on a magnetic substrate*, Phys. Rev. Lett. **71**, 2805–8 (1993).

[26] Calculated by J. Krewer, Blaupunkt-Werke GmbH, Robert-Bosch-Str. 200, D-31139 Hildesheim.

[27] Notice that strict pinning occurs only when the band gap is sufficiently large — much larger than the separation of the quantized levels — and other bands are sufficiently far away. Although many authors arrive at the same equation[8, 9, 10, 11, 28] by different approaches, we think that the geometrical construction used in this figure is particularly transparent.

[28] N.V. Smith, N.B. Brookes, Y. Chang, P.D. Johnson, *Quantum-well and tight-binding analyses of spin-polarized photoemission from Ag/Fe(001) overlayers*, Phys. Rev. B **49**, 332–8 (1994).

[29] D. Kerkmann, D. Pescia, J.W. Krewer, E. Vescovo, *Low energy electron oscillations during epitaxial growth of thin films*, Z. Phys. B **85**, 311–14 (1991).

[30] N.W. Ashcroft, N.D. Mermin *Solid State Physics*, Holt-Saunders International Editions, Tokyo, (1981), p. 170.

[31] G.J. Mankey, R.F. Willis, F.J. Himpsel, *Unoccupied electronic states of ultrathin films of Co/Cu(111) and Fe/Cu(111)*, Phys. Rev. B **47**, 190–6 (1993).

[32] P. Bruno, *Theory of interlayer magnetic coupling*, Phys. Rev. B **52**, 411–39 (1995).

[33] M.D. Stiles, *Exchange coupling in magnetic heterostructures*, Phys. Rev. B **48**, 7238–58 (1993).

[34] D.M. Edwards, J. Mathon, *Oscillations in exchange coupling across a nonmagnetic metallic layer*, J. Magn. Magn. Mat. **93**, 85–8 (1991).

[35] R. Coehoorn, *Period of oscillatory exchange interactions in Co/Cu and Fe/Cu multilayer systems*, Phys. Rev. B **44**, 9331–7 (1991).

[36] V. van Schilfgaarde, W.A. Harrison, *Oscillatory exchange coupling: RKKY or quantum-well mechanism?*, Phys. Rev. Lett. **71**, 3870–3 (1993).

[37] F. Herman, R. Schrieffer, *Generalized Ruderman-Kittel-Kasuya-Yosida theory of oscillatory exchange coupling in magnetic multilayers*, Phys. Rev. B **46**, 5806–9 (1992).

[38] B. Heinrich, J.F. Cochran, M. Kowalewski, J. Kirschner, Z. Celinski, A.S. Arrott, K. Myrtle, *Magnetic anisotropies and exchange coupling in ultrathin FCC Co(001) structures*, Phys. Rev. B **44**, 9348–61 (1991).

[39] P. Grünberg, R. Schreiber, Y. Pang, M.B. Brodsky, H. Sowers, *Layered magnetic structures: evidence for antiferromagnetic coupling of Fe layers across Cr interlayers*, Phys. Rev. Lett. **57**, 2442–5 (1986).

[40] S.S.P. Parkin, N. More, K.P. Roche, *Oscillations in exchange coupling and magnetoresistance in metallic superlattice structures: Co/Ru, Co/Cr, and Fe/Cr*, Phys. Rev. Lett. **64**, 2304–7 (1990).

[41] P. Bruno, C. Chappert, *Oscillatory coupling between ferromagnetic layers separated by a nonmagnetic metal spacer*, Phys. Rev. Lett. **67**, 1602–5 (1991).

[42] $(E_F - E_{AF})/A$ for a realistic Fermi surface: The term in square braces in Eq. 4.2 has to be replaced with $[\kappa_{ij} v_{Fij}]$ were κ_{ij} is the curvature radius of the difference of the two sheets i and j of Fermi survace corresponding the extremal spanning vector and v_{Fij} the reduced Fermi velocities, see [33].

[43] Z.Q. Qiu, J. Pearson, S.D. Bader, *Oscillatory interlayer magnetic coupling of wedged Co/Cu/Co sandwiches grown on Cu(100) by molecular beam epitaxy*, Phys. Rev. B **46**, 8659–62 (1992).

[44] C. Stamm, C. Würsch, S. Egger, D. Pescia, *Amplification of the short-wavelength oscillations in exchange coupled Co-films by low-temperature deposition*, J. Magn. Magn. Mat. **177–181**, 1279–80 (1998).

[45] N.S. Almeida, D.L. Mills, M. Teitelman, *Temperature variation of the interfilm exchange in magnetic multilayers: the influence of spin wave interactions*, Phys. Rev. Lett. **75**, 733–6 (1995).

[46] V. Drchal, J. Kudrnovsky, P. Bruno, I. Turek, P.H. Dederichs, P. Weinberger, *Temperature dependence of the interlayer exchange coupling in magnetic multilayers: An ab initio approach*, Phys. Rev. B **60**, 9588–95 (1999).

[47] J.J. de Vries, A.A.P. Schudelaro, R. Jungblut, P.J.H. Bloemen, A. Reinders, J. Kohlhepp, R. Coehoorn, W.J.M. de Jonge, *Oscillatory interlayer exchange coupling with the Cu cap layer thickness in Co/Cu/Co/Cu(100)*, Phys. Rev. Lett. **75**, 4306–9 (1995).

[48] A. Bounouh, P. Beauvillain, P. Bruno, C. Chappert, R. Megy, P. Veillet, *Theoretical prediction and experimental evidence of a novel oscillatory behaviour of interlayer magnetic coupling*, Europhys. Lett. **33**, 315–20 (1996).

[49] J.S. Helman, W. Baltensperger, *Ruderman-Kittel-Kasuya-Yosida polarization in some inhomogeneous situations*, Phys. Rev. B **50**, 12682–91 (1994).

[50] W. Baltensperger, *Indirect couplings between magnetic layers in a metallic half-space*, J. Magn. Magn. Mat. **198–199**, 415–17 (1999).

[51] A. Rettori, L. Trallori, M.G. Pini, C. Stamm, Ch. Würsch, S. Egger, D. Pescia, *Shifted magnetization curves in ultrathin Co films on stepped Cu(100)*, IEEE Transactions on Magnetics **34**, 1195–7 (1998).

[52] W. Weber, C.H. Back, A. Bischof, D. Pescia, R. Allenspach, *Magnetic switching in cobalt films by adsorption of copper*, Nature **374**, 788–90 (1995).

[53] S.N. Okuno, K. Inomata, *Two oscillatory behaviors as functions of ferromagnetic layer thickness in Fe/Cr(100) multilayers*, Phys. Rev. Lett. **72**, 1553–6 (1994).

[54] S.N. Okuno, K. Inomata, *Oscillatory exchange coupling with a period of two Fe monolayers in Au/Fe/Au/Fe/Au(001)*, Phys. Rev. B **51**, 6139–42 (1995).

[55] P.J.H. Bloemen, M.T.H. van de Vorst, M.T. Johnson, R. Coehoorn, W.J.M. de Jonge, *Magnetic layer thickness dependence of the interlayer exchange coupling in (001) Co/Cu/Co*, Journal of Applied Physics **76**, 7081–3 (1994).

[56] M. Zwierzycki, S. Krompiewski, *Magnetic-sublayers effect on the exchange-coupling oscillations versus cap-layer thickness*, Phys. Rev. B **57**, 5036–9 (1998).

[57] Xiang Dong Zhang, Lie Ming Li, Ye Hong Zhan, Bo Zang Li, Fu Ke Pu, *Angular dependence of the interlayer exchange coupling on the nonmagnetic cap layers*, Chinese Physics Letters **14**, 789–92 (1997).

[58] Xiao Hu, Y. Kawazoe, *Theory of the capping effect in magnetic double-film systems*, Phys. Rev. B **49**, 3294–302 (1994).

[59] P. Bruno, *Interlayer exchange coupling: the role of electron confinement in the overlayer due to the vacuum barrier*, J. Magn. Magn. Mat. **164**, 27–36 (1996).

Curriculum Vitae

25.3.1969	born in St.Gallen (Switzerland)
1976–1985	primary school in Thal (St.Gallen)
1985–1989	apprenticeship as draftsman
1989–1990	working as a draftsman
1991	ETH entrance exam
1991–1996	student of Physics at ETH Zürich, with an exchange year at Dublin City University, Ireland
1996	Diploma in Physics at ETH Zürich
1996–1999	Ph.D. student in the group of Prof. Dr. Danilo Pescia at ETH Zürich

Dank

Die Begeisterung von Danilo Pescia für Physik hat mich immer wieder angesteckt. Viele Diskussionen, seine Hilfe und der kollegiale Stil waren ideale Voraussetzungen. Es hat mir sehr gefallen bei Dir zu doktorieren, vielen Dank!

Bei Hans-Christoph Siegmann möchte ich mich bedanken für sein Interesse an dieser Arbeit und die Übernahme des Koreferats.

Urs Maier hat mir unzählige Male mit Rat und Tat geholfen. Bei kleinen und grösseren Reparaturen und Planungen war ich immer froh um seine breiten Kenntnisse. Danke für Deine Hilfe!

Ohne Christian Back wäre das SPLEED-Experiment undurchführbar gewesen. Danke für Deine Unterstützung! Die Zusammenarbeit war für mich sehr lehrreich.

An die Zeit im Labor mit Christoph Würsch und Christian Stamm denke ich gern zurück. Ich habe da viel von Euch gelernt. Und mit Christian konnte ich bis zum Ende meiner Diss. viele interessante Diskussionen führen. Vielen Dank!

Auch wenn wir selten an den gleichen Projekten arbeiteten, so konnte ich immer auf die Hilfsbereitschaft von Andreas Vaterlaus, Fredy Marty und Urs Ramsperger zählen. Vielen Dank!

Bei Yves Acremann möchte ich mich bedanken für seine unermüdliche Hilfe bei verschiedenen Problemen mit Elektronik und Informatik (z.B. um dies mit LaTeX zu schreiben) und interessante Gespräche.

Besten Dank Mehmet Erbudak, seinen Leuten und der Gruppe Siegmann für ihre Hilfsbereitschaft und das Ausleihen von Material. Bei den Mitarbeitern des Physik-Departements, besonders der Werkstatt, bedanke ich mich für ihre gute Arbeit.